JMEPEG (2024) 33:5563–5569
https://doi.org/10.1007/s11665-023-08319-0


1059-9495/$19.00

TECHNICAL ARTICLE

# Mechanical Properties and Microstructure of Extruded 2198 Al-Li Alloy Bars

*Tian-zhang Zhao, Zhi-xian Fan, Hao-yun Peng, Hong-ran Chen, and Shi-hong Zhang*

Submitted: 12 July 2022 / Revised: 17 March 2023 / Accepted: 6 May 2023 / Published online: 24 May 2023

**Al-Li alloy is widely used in aircraft manufacturing due to its high specific strength. The micro-strengthening mechanisms have been investigated widely, including precipitate and solute strengthening. However, the influence of crystallographic texture on mechanical properties remains unclear, because current researches are based on rolled sheet. In this paper, 2198 Al-Li alloy bars were processed using hot extrusion to obtain a texture different from rolling. The mechanical properties were tested via uniaxial tension. The microstructure was observed using scanning electron microscopy, electron backscattered diffraction, and transmission electron microscopy. The results show that the yielding strength and ultimate tensile strength (UTS) of extruded 2198 Al-Li alloy bars are greatly improved due to the precipitation of $T_1$ precipitate after artificial aging. With the increasing of pre-deformation, the number of $T_1$ increases, and the size of $T_1$ precipitate is close to each other, leading to a remarkable increase in strength. When the pre-deformation is 6%, the UTS reaches 611 MPa. 2198 Al-Li alloy bars possess two types of fiber textures: <100> // extrusion direction and <111> // extrusion direction. The presence of <111> fibrous texture with a low Schmid factor can increase the strength of extruded 2198 Al-Li alloy bars. The fracture mechanism of the bar is ductile fracture after artificial aging, while the fracture mechanism is a mix of micropore aggregation and cleavage after natural aging.**

**Keywords** Al-Li alloy, crystallographic texture, extrusion, precipitation

## 1. Introduction

Al-Li alloys are favored by the aerospace industry due to their unique advantages, such as low density, high specific strength, and low fatigue crack growth rate. The application of advanced Al-Li alloy can not only reduce the weight of the aircraft structure but also substantially decrease flight costs (Ref 1-3). 2198 Al-Li alloy, a third-generation Al-Li alloy, is crucial for realizing the lightweight nature of modern aircraft.

As an age-hardenable alloy, the mechanical properties of 2198 Al-Li alloy are mainly determined by the microstructure of the second phase. The influences of heat treatment on the mechanical properties and microstructure of 2198 Al-Li alloy have been reported in recent literature. Dorin et al. (Ref 4) performed different heat treatments on 2198 Al-Li alloy sheets and established a strengthening model based on interface strengthening and stacking fault strengthening. Chen et al. (Ref 5) found that the fracture path of 2198 Al-Li alloy sheets mainly depends on loading direction. Zhang et al. (Ref 6) investigated the tensile properties, hardness, and electrical conductivity of 2198 Al-Li alloy sheets, which vary regularly with aging temperature. At present, most of the investigations about 2198 Al-Li alloy focus on rolled sheets. Examilioti et al. (Ref 7) revealed that the anisotropy of 2198 Al-Li alloy is more obvious under the $T_3$ state, and an anisotropic analytical model was established considering different strengthening precipitates (Ref 8). The $T_1$ precipitate with a hexagonal structure plays an important role in the strengthening of 2198 Al-Li alloy. Noble et al. (Ref 9, 10) confirmed that the increase in modulus is mainly contributed by lithium addition, and $T_1$ precipitates are on the {111} planes with the orientation relationship: $(0001)_{T1}//(111)_{Al}$, $(10-10)_{T1}//(1-10)_{Al}$, and $(11-20)_{T1}//(2-1-1)_{Al}$. It has been observed via high-resolution transmission electron microscopy (HRTEM) that $T_1$ precipitate can be sheared by dislocations (Ref 11-13). Nie et al. (Ref 14) established a shearing model and described the evolution of yielding strength successfully. Li et al. (Ref 15) established a prediction model based on the Hosford theory, which can describe the tension-compression strain accurately. Thus, many studies have investigated the relationship between the precipitates and strength.

However, the contribution of crystallographic texture to the strengthening is unclear. Hot extrusion is a usually used method to obtain a different texture from sheets. Chen et al. (Ref 16-18) revealed the influence of extrusion and heat treatment on the microstructure and mechanical properties of 2196 Al-Li alloy. Liu et al. (Ref 19) measured the springback of 2196 Al-Li alloy after bending and established an analytical model based on the strain neutral layer. Xu et al. (Ref 20) observed that S'/S and $T_2$ phases usually precipitated in the abnormal grain growth areas. Sun et al. (Ref 21) studied the effect of shot peening on the microstructure and mechanical properties of 2196 Al-Li alloy. After extrusion, 2195 Al-Li alloy forms a typical incomplete recrystallized structure with an obvious texture (Ref 22-24).

**Tian-zhang Zhao, Zhi-xian Fan,** and **Hong-ran Chen**, Shenyang Aerospace University, Shenyang 110136, China; **Hao-yun Peng**, AVIC Shenyang Aircraft Industry (Group) Co. Ltd, Shenyang 110034, China; and **Shi-hong Zhang**, Institute of Metal Research, Chinese Academy of Sciences, Shenyang 110016, China. Contact e-mail: 137411635@qq.com.

Copper texture may be the main reason for the strength anisotropy of extruded 2195 Al-Li alloy (Ref 25). Ma et al. (Ref 26) evaluated that the nucleation time of $T_1$ precipitate in 2195 Al-Li alloy after extrusion is short, and the precipitation distribution is uneven. It can be found that the extrusion process has important influences on the microstructure and mechanical properties of Al-Li alloys.

The crystallographic texture, pre-deformation, and precipitation form a complex system that determines the strengthening of 2198 Al-Li alloy during artificial aging. However, how the mechanical properties and strengthening mechanism vary is unclear when the crystallographic texture changes. In the present work, the hot extrusion experiment of as-cast 2198 Al-Li alloy was first performed. Then, the mechanical properties of extruded 2198 Al-Li alloy bars under different conditions were tested. Meanwhile, the crystallographic texture and precipitate morphology were observed using EBSD and TEM. Finally, fracture mechanisms under different conditions were analyzed. We hope that it can help to understand the relationship between processing, mechanical properties, and microstructure of 2198 Al-Li alloy.

## 2. Materials and Methods

The material used in this experiment was as-cast 2198 Al-Li alloy. Table 1 reveals the chemical composition of 2198 Al-Li alloy. The as-cast alloy ingot was homogenized at 500 °C for 48 h and then cooled to room temperature with a furnace. The diameter of the initial ingot was 128 mm. The diameter of the extrusion container was 140 mm, and the diameter of the bar after extrusion was 75 mm. The billet and container were heated together to 500 °C. Then, hot extrusion was performed with a 3.5:1 extrusion ratio at a loading rate of 2 mm/s.

The tensile tests along the extrusion direction were carried out on MTS tester with a strain rate of $4 \times 10^{-4}$ $s^{-1}$. The processing route and positions of tensile specimens taken at the same radius are shown in Fig. 1. After solution treatment at 510 °C for 1.5 h and water quenching, a plastic pre-deformation was applied to the samples immediately. Then, the samples were naturally aged for 7 days and artificially aged at 155 °C for 15 h. The surfaces of tensile fracture under different conditions were observed using SEM.

The crystallographic texture was measured using EBSD on an FEI Nova Nano scanning electron microscope. The EBSD samples were prepared by standard grinding, polishing, and electrochemical polishing. The conditions for electrochemical polishing were 20 V, room temperature, and 7 vol.% of perchloric acid in ethanol. TEM was employed to observe precipitates after artificial aging, which was performed on an FEI Tecnai G2 F30 TEM. The conditions for twin-jet electropolishing were − 30 °C, 38 V, and 7% perchloric acid in ethanol.

## 3. Results and Discussion

### 3.1 Mechanical Properties

The true stress–strain curves of extruded 2198 Al-Li alloy bars under different conditions are shown in Fig. 2a. The yielding strength (YS), ultimate tensile strength (UTS), and uniform elongation are compared in Fig. 2b. The YS and UTS are only 339 and 557 MPa after natural aging. The reason is that the main strengthening phase of 2198 Al-Li alloy after natural aging is δ'. The strengthening effect is limited because δ' is coherent with the matrix (Ref 27, 28). When the pre-deformation before artificial aging is 0%, the YS and UTS after artificial aging increase to 434 and 562 MPa, respectively. However, the uniform elongation decreases from 13.3 to 8.7%. This is because the precipitation of the $T_1$ precipitate leads to an increase in strength and a decrease in elongation (Ref 6, 12). The YS and UTS increase with the increasing of pre-deformation. When pre-deformation is 6%, YS and UTS reach 560 MPa and 611 MPa, respectively. The increase in strengthening results has two causes: strain hardening during pre-deformation and precipitation strengthening. And the strengthening from $T_1$ precipitate is dominant (Ref 29).

Figure 2c shows the Kocks–Mecking plot (Ref 30, 31) (work hardening rate $\theta = d\sigma/d\varepsilon$) of extruded 2198 Al-Li alloy bars

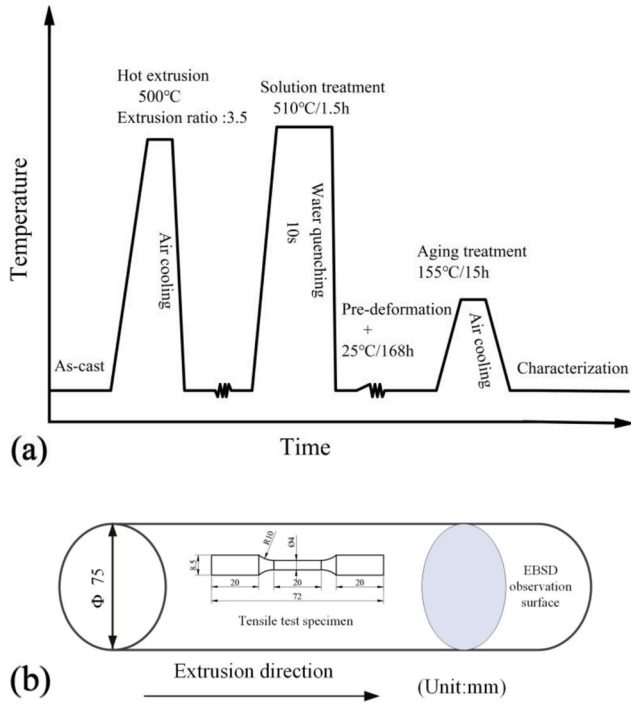


**Fig. 1** (a) Processing route of extruded 2198 Al-Li alloy bars and (b) dimensions and sampling locations of the tensile specimens after extrusion

**Table 1 Chemical compositions (wt.%) of 2198 Al-Li alloy**

| Cu | Li | Zn | Mn | Mg | Zr | Si | Ag | Fe | Al |
|---|---|---|---|---|---|---|---|---|---|
| 2.9-3.5 | 0.8-1.1 | ≤ 0.35 | ≤ 0.5 | 0.25-0.8 | 0.04-0.18 | ≤ 0.08 | 0.1-0.5 | ≤ 0.01 | Bal |

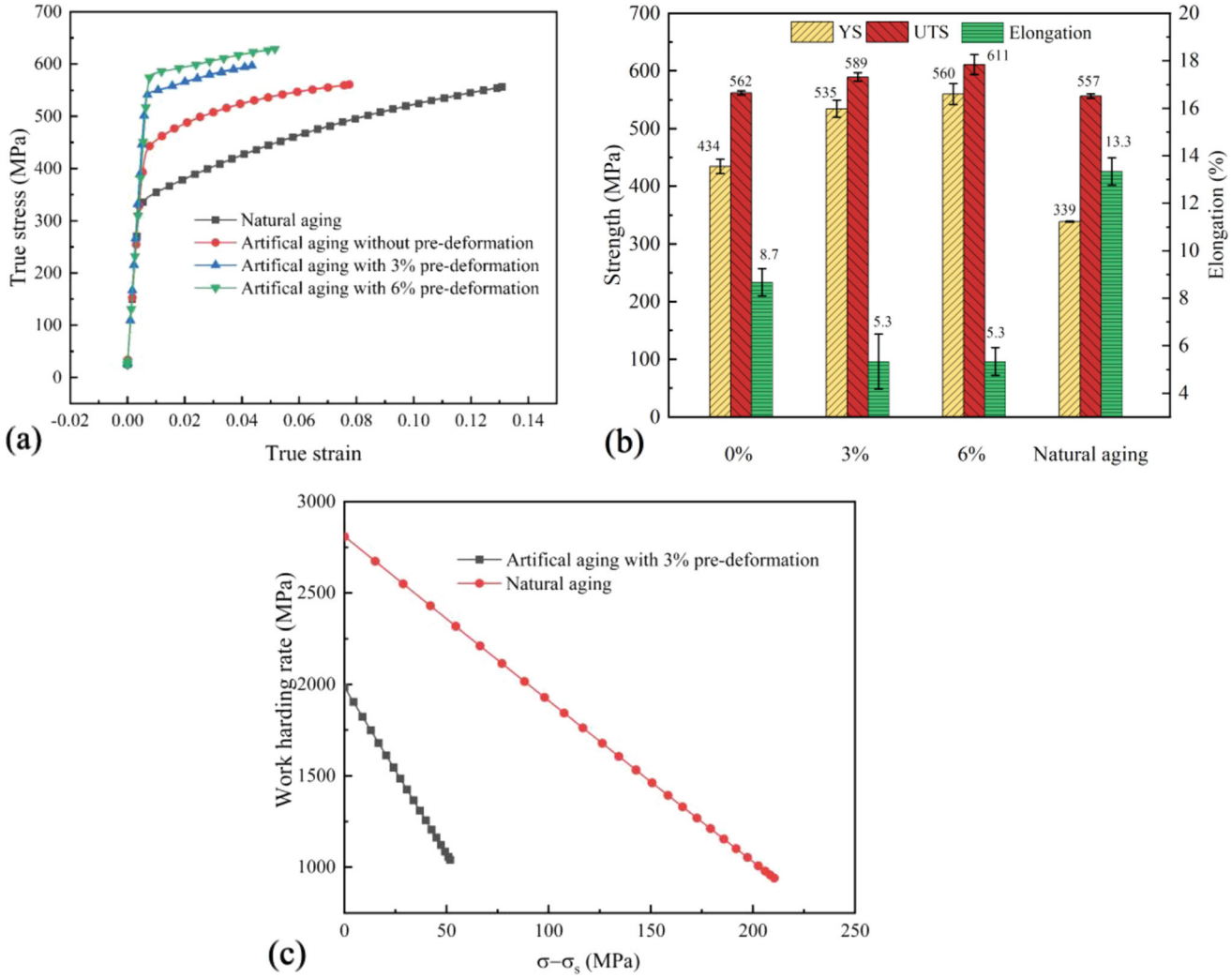


**Fig. 2** Mechanical properties of extruded 2198 Al-Li alloy bars under different aging conditions: (a) true stress–strain curve; (b) yielding strength, ultimate tensile strength, and uniform elongation; and (c) work hardening rate

after natural aging and artificial aging with 3% pre-deformation. The initial work hardening after natural aging, approximately 2809 MPa, is much higher than that after artificial aging. Although both work hardening rates decrease with the increasing of stress, the decreasing rate is different. A similar phenomenon can be found by Deschamps (Ref 31). The high hardening rate is due to dynamic precipitation, solute affects the dislocation/dislocation junctions (Ref 32, 33). The initial hardening rate can be expressed as follows (Ref 34): $\theta_0 = \frac{M^2 \alpha \mu b k_1}{2}$ where $M$ is the Taylor factor, $\mu$ is the shear modulus, $b$ is the Burgers vector, $k_1$ is the efficiency with which a dislocation junction will form from a random encounter between moving dislocations, and $\alpha$ is proportional to the stress necessary to break a dislocation junction. The interactions between dislocations and $T_1$ precipitate change from shearing to the by-passing mechanism with the increasing of $T_1$ thickness. However, the δ' phases and Cu clusters produced after natural aging affect shear modulus and dislocation junction strength, resulting in a high hardening rate.

### 3.2 Crystallographic Texture

Since the preferred crystallographic orientation is a very important factor for strengthening, EBSD was used to measure the grain orientations of extruded 2198 Al-Li alloy bars. Figure 3a shows the grain orientation map of extruded 2198 Al-Li alloy bars (observation plane is perpendicular to extrusion direction) showing that there are a lot of sub-grain boundaries and fine recrystallized grains. Two primary different crystallographic orientations (blue and red) can be seen, with volume percent of 57.6 and 33.4%, respectively. The average size of the grains is 23.6 $\mu$m, as shown in Fig. 3b. Small-sized grains account for the majority, according to the famous Hall–Petch relationship (Ref 35), which is conducive to the improvement of strength. Figure 3c reveals grain boundaries, in which red and green represent low-angle grain boundaries (LAGBs) and high-angle grain boundaries (HAGBs), respectively. Most of the boundaries are LAGBs with a frequency of 75% (Fig. 3d).

The pole figure and schematic diagram of crystal distribution of extruded 2198 Al-Li alloy bars are shown in Fig. 4. There are two main types of crystallographic texture: <111> fiber texture and <100> fiber texture parallel to the extrusion direction. Figure 5a exhibits the distribution of the Schmid factor of the extruded bar when it is stretched along the extrusion direction. The frequency has two peaks, and the average Schmid factor is 0.37, as shown in Fig. 5b. According to Schmid's law (Ref 36), it is known that the slipping system

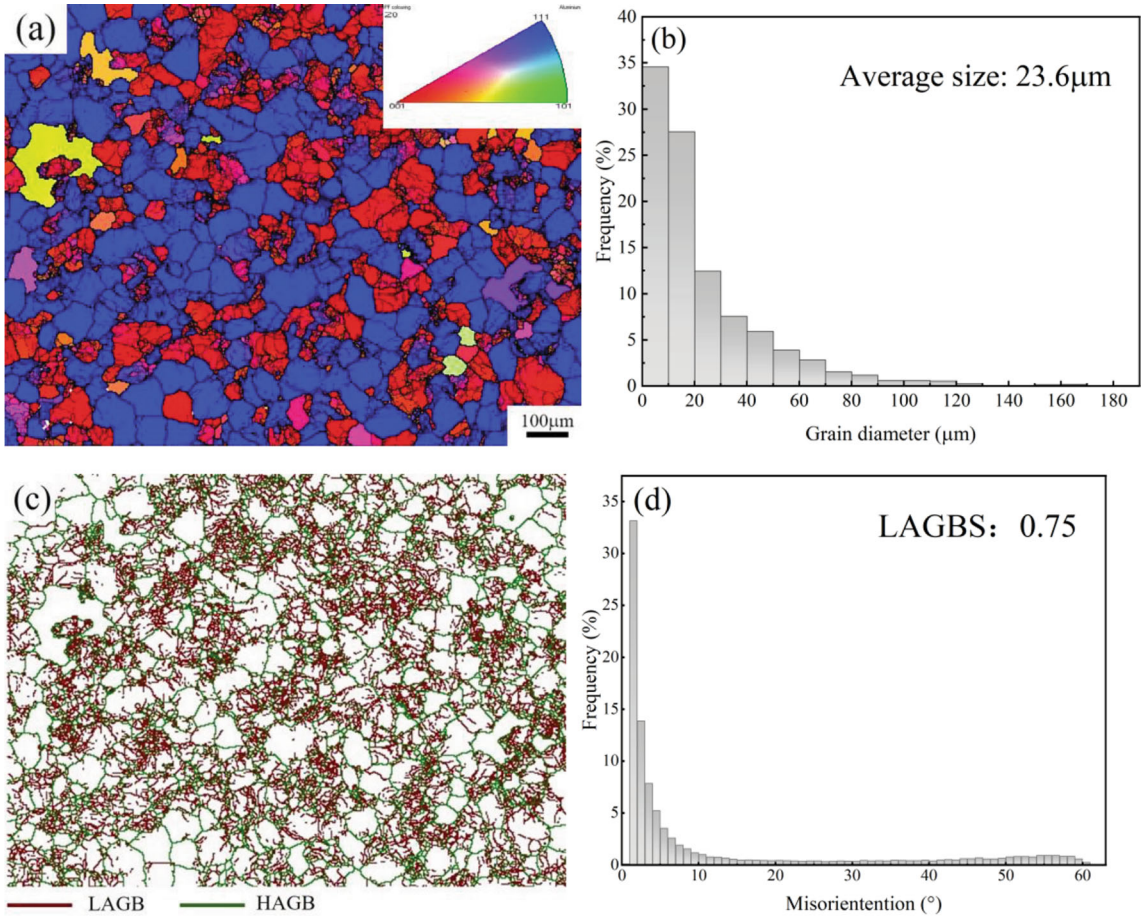


**Fig. 3** EBSD maps of extruded 2198 Al-Li alloy bars: (a) grain orientation map; (b) grain size distribution; (c) grain boundary map; and (d) misorientation angle distribution

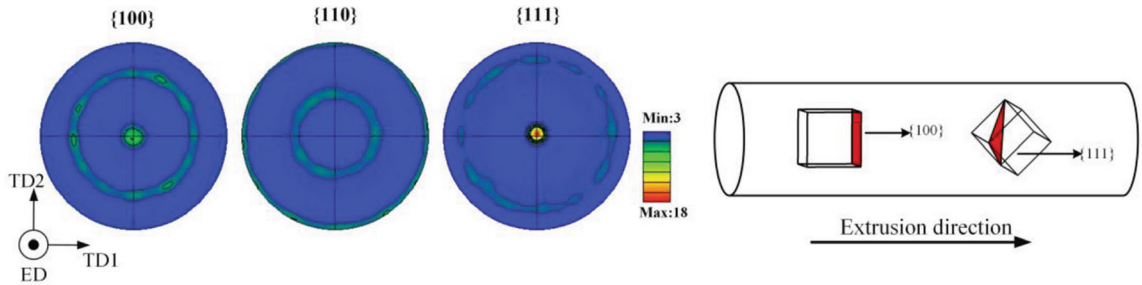


**Fig. 4** Pole figure and schematic diagram of crystal distribution of extruded 2198 Al-Li alloy bars

with a higher Schmid factor can be activated easier. Thus, the presence of <111> fibrous texture with a low Schmid factor can increase the strength of extruded 2198 Al-Li alloy bars.

### 3.3 Precipitates

In order to further study the effect of precipitates on the mechanical properties of extruded 2198 Al-Li alloy bars, TEM images in <110> matrix zone axis are used to observe the microstructure after artificial aging. When the pre-deformation is 0%, there are few δ' and a small amount of $T_1$ precipitates, as shown in Fig. 6a. The frequency distribution of $T_1$ precipitates diameter is given in Fig. 6b, and the average diameter of $T_1$ precipitates is about 135.4 nm. The amount of $T_1$ precipitates increases, and the diameter decreases with the increasing of pre-deformation, as shown in Fig. 6c, d, e, and f. Additionally, the size of $T_1$ precipitates is close to each other with the increasing of pre-deformation. The pre-deformation provides nucleation points for $T_1$ precipitates, which can improve the precipitation kinetics and number density of $T_1$ precipitates (Ref 10). Therefore, when the pre-deformation is 6%, the amount of $T_1$ precipitates is the largest, and the average diameter, 67.2 nm, is the smallest. It is the reason why the strength of extruded 2198 Al-Li alloy bars increases with the increasing of pre-deformation.

### 3.4 Fracture Mechanism

Figure 7a shows the tensile fracture morphology of extruded 2198 Al-Li alloy bars after artificial aging. The inserted figure in the upper right corner is the macroscopic fracture,

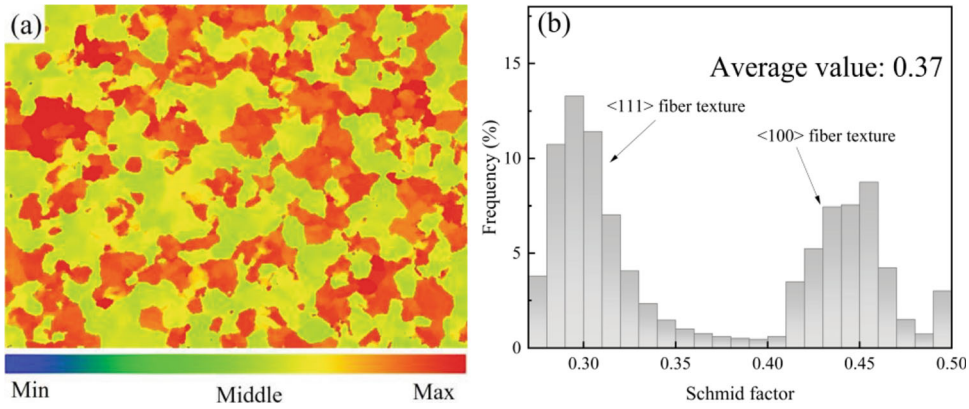


**Fig. 5** (a) Schmid factor distribution and (b) frequency of Schmid factor of extruded 2198 Al-Li alloy bars

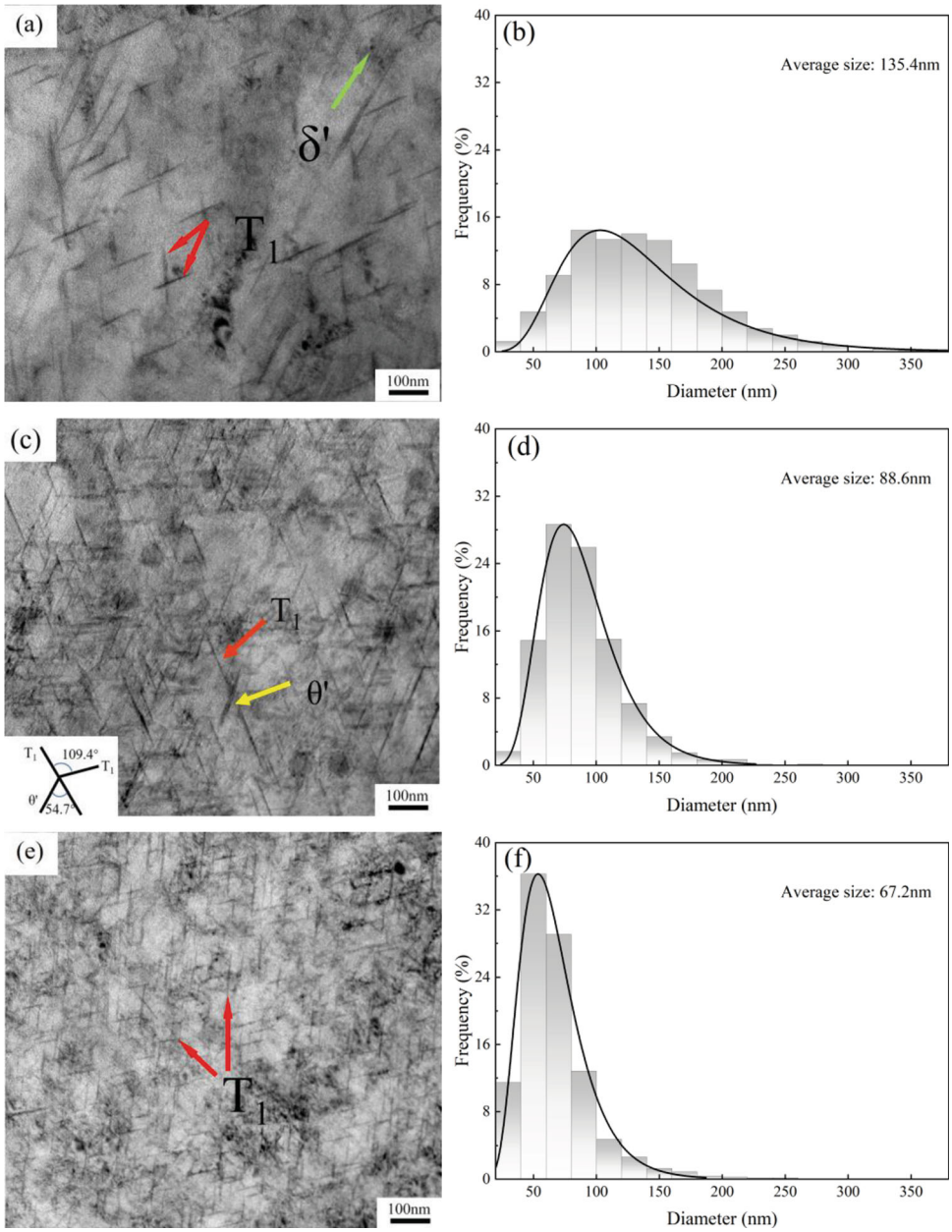


**Fig. 6** TEM images in < 110 > matrix zone axis and $T_1$ diameter distribution maps of extruded 2198 Al-Li alloy bars with different pre-deformations (a) (b) 0%; (c) (d) 3%; and (e) (f) 6%

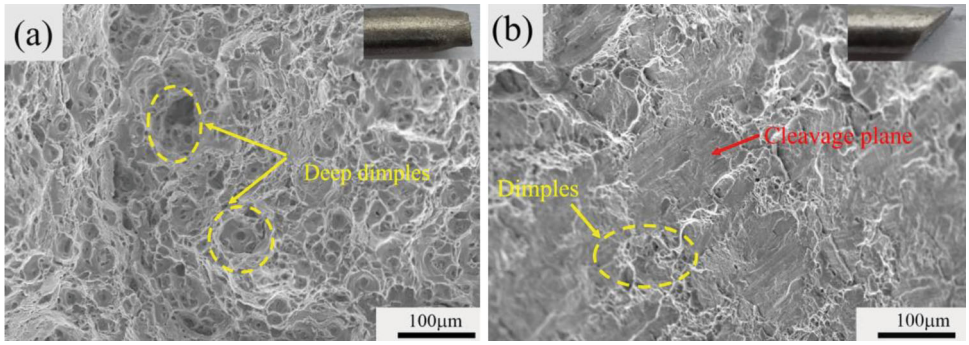


**Fig. 7** Tensile fracture morphology of extruded 2198 Al-Li alloy bars after (a) artificial aging with 3% pre-deformation and (b) natural aging

indicating an obvious necking phenomenon. The microscopic fracture surface consists of many equiaxed dimples, which proves that the fracture mechanism is micropore aggregation. The fracture surface of extruded 2198 Al-Li alloy bars after natural aging is revealed in Fig. 7b. There is no obvious necking, and only a few dimples can be seen. In addition, a lot of cleavage planes appear. Hence, the fracture mechanism after natural aging is a mixture of micropore aggregation and cleavage. Although there are more dimples on the fracture surface of the artificially aged samples than the naturally aged, its uniform elongation is lower. This is because the work hardening rate of extruded 2198 Al-Li alloy bars after natural aging is much higher than that after artificial aging, as analyzed in Sect. 3.1. The higher hardening ability can make the strain distribution more homogeneous. Thus, the necking is delayed, and the uniform elongation increases.

## 4. Conclusions

In this study, the mechanical properties of extruded 2198 Al-Li alloy bars were tested. SEM, EBSD, and TEM were used to observe the fracture morphology, crystallographic texture, and precipitates. The conclusions can be drawn as follows:

(1) The extruded 2198 Al-Li alloy bars have higher strength than the sheets reported in the literature. With the increasing of pre-deformation, YS and UTS gradually increase. When the pre-deformation is 6%, the UTS reaches 611 MPa.
(2) The high strength of extruded 2198 Al-Li alloy bars stems from four aspects: small grain size ($< 23.6\ \mu m$), a large number of LAGBs ($> 75\%$), a large amount of $T_1$ after artificial aging, and strong extruded $<111>$ fiber texture.
(3) After natural aging, the fracture mechanism is a mix of micropore aggregation and cleavage. The fracture mechanism changes to ductile fracture dominated by dimples after artificial aging. However, it has a higher uniform elongation after natural aging, due to having higher work hardening rate.

### Acknowledgments

The financial supports of National Natural Science Foundation of China (No: 51605310), Foundation of Liaoning Educational Committee (No: LJKZ0180), and Plan for Young and Middle-aged Innovators of Shenyang (No: RC210422) are gratefully acknowledged.

### References

1. E.J. Lavernia, T.S. Srivatsan, and F.A. Mohamed, Strength, Deformation, Fracture Behaviour and Ductility of Aluminium-Lithium Alloys, *J. Mater. Sci.*, 1990, **25**, p 1137–1158
2. J.C. Williams and E.A. Starke, Progress in Structural Materials for Aerospace Systems, *Acta Mater.*, 2003, **51**, p 5775–5799
3. T. Warner, Recently-Developed Aluminium Solutions for Aerospace Applications, *Mater. Sci. Forum.*, 2006, **519–521**, p 1271–1278
4. T. Dorin, A. Deschamps, F.D. Geuser, and C. Sigli, Quantification and Modeling of the Microstructure/Strength Relationship by Tailoring the Morphological Parameters of the $T_1$ Phase in an Al-Cu-Li alloy, *Acta Mater.*, 2014, **75**, p 134–146
5. J.Q. Chen, Y. Madi, T.F. Morgeneyer, and J. Besson, Plastic Flow and Ductile Rupture of a 2198 Al-Cu-Li Aluminum Alloy, *Comp. Mater Sci.*, 2011, **50**, p 1365–1371
6. S.F. Zhang, W.D. Zeng, W.H. Yang, C.L. Shi, and H.J. Wang, Ageing Response of a Al-Cu-Li 2198 Alloy, *Mater. Des.*, 2014, **63**, p 368–374
7. T.N. Examilioti, B. Klusemann, N. Kashaev, S. Riekehr, J. Enz, and N.D. Alexopoulos, Anisotropy and Size Effect in Tensile Mechanical Properties of Al-Cu-Li 2198 Alloy, *Struct. Integr. Procedia.*, 2017, **5**, p 13–18
8. T.Z. Zhao, L. Jin, Y. Xu, and S.H. Zhang, Anisotropic Yielding Stress of 2198 Al-Li Alloy Sheet and Mechanisms, *Mater. Sci. Eng. A.*, 2020, **771**, p 138572
9. B. Noble, S.J. Harris, and K. Dinsdale, The Elastic Modulus of Aluminium-Lithium Alloys, *J. Mater. Sci.*, 1982, **17**, p 461–468
10. B. Noble and G.E. Thompson, $T_1$ ($Al_2CuLi$) Precipitation in Aluminium-Copper-Lithium Alloys, *Met. Sci. J.*, 1972, **6**, p 167–174
11. J.M. Howe, J. Lee, and A. Vasudévan, Structure and Deformation Behavior of $T_1$ Precipitate Plates in an Al-2Li-1Cu Alloy, *Metall. Trans. A.*, 1988, **19**, p 2911–2920
12. T. Dorin, F.D. Geuser, W. Lefebvre, C. Sigli, and A. Deschamps, Strengthening Mechanisms of $T_1$ Precipitates and Their influence on the Plasticity of an Al-Cu-Li Alloy, *Mater. Sci. Eng. A.*, 2014, **605**, p 119–126
13. Y.J. Deng, J.H. Bai, X.D. Wu, G.J. Huang, L.F. Cao, and L. Huang, Investigation on Formation Mechanism of $T_1$ Precipitate in an Al-Cu-Li Alloy, *J. Alloys. Compd.*, 2017, **723**, p 661–666
14. J.F. Nie and B.C. Muddle, Microstructural Design of High-Strength Aluminum Alloys, *J. Phase. Equilib.*, 1998, **19**, p 543–551
15. X.Q. Li, N. Song, G.Q. Guo, and Z.G. Sun, Prediction of Forming Limit Curve (FLC) for Al-Li Alloy 2198-T3 Sheet using Different Yield Functions, *Chin. J. Aeronaut.*, 2013, **26**, p 1317–1323
16. X.X. Chen, X.W. Ma, H.K. Xi, G.Q. Zhao, Y.X. Wang, and X.X. Xu, Effects of Heat Treatment on the Microstructure and Mechanical Properties of Extruded 2196 Al-Cu-Li Alloy, *Mater. Des.*, 2020, **192**, p 108746
17. X.X. Chen, G.Q. Zhao, G.L. Liu, L. Sun, L. Chen, and C.S. Zhang, Microstructure Evolution and Mechanical Properties of 2196 Al-Li

Alloy in Hot Extrusion Process, *J. Mater. Process. Technol.*, 2020, **275**, p 116348
18. X.X. Chen, G.Q. Zhao, X. Xu, and Y.X. Wang, Effects of Heat Treatment on the Microstructure, Texture and Mechanical Property Anisotropy of Extruded 2196 Al-Cu-Li Alloy, *J. Alloys. Compd.*, 2021, **862**, p 158102
19. T.J. Liu, Y.J. Wang, J.J. Wu, X.J. Xia, J.B. Wang, W. Wang, and S.H. Wang, Springback Analysis of Z & T-Section 2196-T8511 and 2099-T83 Al-Li Alloys Extrusions in Displacement Controlled Cold Stretch Bending, *J. Mater. Process. Technol.*, 2015, **225**, p 295–309
20. X. Xu, X.W. Ma, G.Q. Zhao, Y.X. Wang, and X.X. Chen, Effects of Abnormal Grain Growth at Longitudinal Weld on the Aging Behavior and Mechanical Properties of 2196 Al-Cu-Li Alloy Profile, *Mater. Des.*, 2021, **210**, p 110043
21. B.L. Sun, Y.J. Wang, J.Y. Xiao, G.Q. Gao, M.J. Qiao, and X.D. Xiao, Evolution of Microstructure and Properties of 2196 Al-Li Alloy Induced by Shot Peening, *Procedia. Eng.*, 2014, **81**, p 1043–1048
22. Y.X. Wang, G.Q. Zhao, X. Xu, X.X. Chen, and W.D. Zhang, Microstructures and Mechanical Properties of Spray Deposited 2195 Al-Cu-Li Alloy Through Thermo-Mechanical Processing, *Mater. Sci. Eng. A.*, 2018, **727**, p 78–89
23. C.S. Zhang, M.F. Liu, Z.J. Meng, Q.Y. Zhang, G.Q. Zhao, L. Chen, H. Zhang, and J. Wang, Microstructure Evolution and Precipitation Characteristics of Spray-Formed and Subsequently Extruded 2195 Al-Li Alloy Plate During Solution and Aging Process, *J. Mater. Process. Technol.*, 2020, **283**, p 116718
24. Q. Li, J. Ning, L. Chen, J.L. Hu, and Y.X. Liu, The Mechanical Response and Microstructural Evolution of 2195 Al-Li Alloy During Hot Tensile Deformation, *J. Alloys Compd.*, 2020, **848**, p 156515
25. J.M. Dickson and T.H. Sanders, Crystallographic Texture Development in Extruded AA 2195 and AA 7075, *Mater. Charact.*, 2020, **160**(10), p 110121
26. Y.L. Ma, J.F. Li, R.Z. Zhang, J.G. Tang, C. Huang, H.Y. Li, and Z.Q. Zheng, Strength and Structure Variation of 2195 Al-Li Alloy Caused by Different Deformation Processes of Hot Extrusion and Cold-Rolling, *Trans. Nonferrous Met. Soc. China.*, 2020, **30**(4), p 835–849
27. R. Yoshimura, T.J. Konno, E. Abe, and K. Hiraga, Transmission Electron Microscopy Study of the Early Stage of Precipitates in Aged Al-Li-Cu Alloys, *Acta Mater.*, 2003, **51**(10), p 2891–2903
28. S. Wang, J.S. Wang, C. Zhang, and C. Xue, Continuous Precipitate Modes of the δ'-$Al_3Li$ Phase in Al-Li Alloys, *J. Alloys. Compd.*, 2022, **904**, p 163800
29. B.I. Rodgers and P.B. Prangnell, Quantification of the Influence of Increased Pre-stretching on Microstructure-strength Relationships in the Al-Cu-Li Alloy AA2195, *Acta mater.*, 2016, **108**, p 55–67
30. U.F. Kocks, Laws for Work-Hardening and Low-Temperature Creep, *J. Eng. Mater. Tech.*, 1976, **98**, p 76–85
31. A. Deschamps, B. Decreus, F. De Geuser, T. Dorin, and M. Weyland, The Influence of Precipitation on Plastic Deformation of Al-Cu-Li Alloys, *Acta Mater.*, 2013, **61**, p 4010–4021
32. J.D. Costa Teixeira, Y. Brechet, Y. Estrin, and C. Hutchinson, The Strain Hardening Behaviour of Supersaturated Al-Cu alloys, In Proceedings of the 12th International Conference on Aluminium Alloys., 2010 (Japan), p 536–541
33. A. Deschamps, F. Bley, F. Livet, and D. Fabregue, In-situ Small-angle X-ray Scattering Study of Dynamic Precipitation in an Al-Zn-Mg-Cu Alloy, *Philos Mag.*, 2003, **83**(6), p 677–692
34. U.F. Kocks and H. Mecking, Physics and Phenomenology of Strain Hardening: the FCC Case, *Prog Mater Sci.*, 2003, **48**(3), p p171-273
35. N. Hansen, Hall-Petch Relation and Boundary Strengthening, *Scr. Mater.*, 2004, **51**, p 801–806
36. J. Cho, J.F. Molinari, and G. Anciaux, Mobility Law of Dislocations with Several Character Angles and Temperatures in FCC Aluminum, *Int. J. Plast.*, 2017, **90**, p 66–75